Robustness of quantum gates with hybrid spin-photon qubits in superconducting resonators

A. Chiesa,[1] D. Gerace,[2] F. Troiani,[3] G. Amoretti,[1] P. Santini,[1] and S. Carretta[1]
[1]*Dipartimento di Fisica e Scienze della Terra, Università di Parma, I-43124 Parma, Italy*
[2]*Dipartimento di Fisica, Università di Pavia, via Bassi 6, I-27100 Pavia, Italy*
[3]*S3 Istituto Nanoscienze, Consiglio Nazionale delle Ricerche, I-41100 Modena, Italy*
(Received 21 February 2014; published 9 May 2014)

We discuss a scalable scheme for the implementation of quantum-information processing in qubits formed by superconducting resonators and spin ensembles. The scheme is based on a hybrid dual-rail encoding, which allows one to perform both single- and two-qubit gates by shifting the resonator frequency. We estimate the quantum-gate fidelity by simulating the driven dynamics through a master-equation approach. High values of the fidelity can be achieved also in the presence of the main decoherence sources, namely, cavity-photon loss, and pure dephasing of the superconductive elements that are involved in the two-qubit gates. This result allows envisioning the scalability of such elements to a quantum-computing architecture made of an array of hybrid spin-photon qubits. Analogous results are obtained for a simpler, nonscalable setup, which we propose here in order to simplify the realization of the first proof-of-principle experiments.

DOI: 10.1103/PhysRevA.89.052308 PACS number(s): 03.67.Lx, 42.50.Pq, 75.50.Xx

I. INTRODUCTION

Superconducting circuits are emerging as promising candidates for the realization of scalable quantum-information processing [1,2]. In the context of so-called *circuit-quantum electrodynamics* [3], an important achievement is represented by the strong coupling between microwave photons confined in a superconducting resonator and superconducting qubits [4]. The strong anharmonicity provided by these artificial atoms allows one to control the number of photonic excitations introduced in the resonator [5]. Ideally, they should also show long coherence times to perform many quantum gates at high speed [6], which could be exploited in a prospective scalable architecture for quantum computation [7]. However, highly anharmonic superconducting qubits are usually more affected by dissipation [8]. Even though important advances have been made to increase the coherence times of superconducting qubits [9], other physical systems, such as spin ensembles (SEs), would provide much more stability.

For these reasons, hybrid devices are being investigated [10–15], in order to benefit from the fast manipulation rates of superconducting qubits, such as Cooper-pair boxes (CPBs) or transmons [1,4,6,7,16], while avoiding the limitations coming from their relaxation and dephasing mechanisms [8,9]. In such devices, superconducting qubits and spin ensembles are used, respectively, to process and store quantum information, while cavity photons induce an effective coupling between them, thus acting as a quantum bus [17,18]. In order to use the SE as a quantum memory, its coupling with the resonator mode has to exceed the dephasing and relaxation rates in the system. With this aim, a $\sqrt{N}$ enhancement of the spin-photon coupling is achieved by replacing single-spin excitations with the collective excitations of the spin ensemble, N being the number of coupled spins. This allowed the achievement of coupling constants in the megahertz range with nitrogen vacancy defects in diamond [19], and Cr^{3+} spins in Al_2O_3 [20]. On the other hand, a significant reduction of the photon-loss rate is achieved in resonators with high quality factor (Q). Great improvements in increasing Q have recently been demonstrated, leading to the realization of superconducting resonators [21] reaching experimental $Q \sim 10^6$–10^7.

Based on the same ingredients and experimental achievements, we have recently proposed a different approach for the implementation of quantum-information processing [22]. This is based on a hybrid dual-rail encoding of the qubit, in which both photonic and spin degrees of freedom enter on an equal footing. As a result, quantum gates can be implemented by a single tool, namely, by tuning the resonator frequencies. This can be achieved, e.g., by external magnetic fields [23] or by means of micro superconducting quantum interference devices properly connected to the resonator [24,25]. A single qubit is encoded in each cavity and an additional cavity contains a superconducting device (a CPB) which is exploited as an auxiliary degree of freedom to implement two-qubit gates. As the CPB is excited only during the implementation of two-qubit gates, its possibly short coherence time should not introduce significant error rates.

In order to assess the feasibility of the proposed approach in relation to the state-of-the-art technology, it is important to gain a quantitative understanding of the main decoherence processes and of their effect on the quantum gates. In the present work, we report a detailed study of the effects of relaxation and dephasing on the system dynamics, by simulating the quantum gates within a master-equation formalism. Such decoherence channels are considered for each element involved in the quantum computation, namely, photons, SEs, and the CPB. We find that the most important source of error is given by photon loss. However, for reasonably high (but technologically achievable) values of the quality factor ($Q \approx 10^5$–10^6), one can reach high values of the quantum-gate fidelity (>95%).

The paper is organized as follows. Section II contains a brief description of the qubit encoding in the scalable setup, of the model Hamiltonian, and of the implementation of the single- and two-qubit quantum gates. Section III is devoted to the description of the density matrix formalism that is used to simulate the quantum gates, and to the estimate of the gate fidelity in the presence of decoherence. In Sec. IV we describe a nonscalable setup, which could simplify the realization of

the first proof-of-principle experiments. Finally, in Sec. V we discuss different aspects of the scheme implementation, and in Sec. VI we draw the conclusions.

II. DESCRIPTION OF THE SCALABLE SETUP

A set of gates is said to be universal for quantum computation if any unitary operation may be performed by means of a quantum circuit involving only those gates. We describe here such a set, consisting of a controlled-Z (CZ) two-qubit gate and of arbitrary single-qubit rotations around two nonparallel axes [26]. In particular, we summarize the hybrid qubit encoding already introduced in Ref. [22], as well as the setup, the model Hamiltonian, and the scheme adopted for the quantum-gate implementation.

A. Hybrid dual-rail qubit encoding

We consider a coplanar waveguide resonator containing a single photon in a mode of frequency ω_c, and an ensemble of N noninteracting $s = 1/2$ spins, each prepared in its ground state: $|\psi_0\rangle \equiv |\downarrow_1 \cdots \downarrow_N\rangle$. The spins can be initialized in the state $|\psi_0\rangle$, e.g., by cooling them down in a static magnetic field. If the resonator frequency is tuned to match the spin gap ω, the SE can absorb the photon and collectively evolve into the state $|\psi_1\rangle = \frac{1}{\sqrt{N}} \sum_{q=1}^{N} |\downarrow_1 \cdots \uparrow_q \cdots \downarrow_N\rangle$ [27]. Spin excitations are described (in the limit of a small number of excitations) by the bosonic operators $\hat{b}$ and $\hat{b}^\dagger$, where $\hat{b} = \frac{1}{\sqrt{N}} \sum_{q=1}^{N} |\downarrow\rangle\langle\uparrow|_q$ and $[\hat{b},\hat{b}^\dagger] = 1$ [15,19]. Within the single-excitation subspace of the system formed by the cavity mode and the SE, we introduce the hybrid dual-rail encoding of the qubit μ:

$$\begin{aligned} |0\rangle_\mu &\equiv \hat{b}_\mu^\dagger |\emptyset\rangle = \left|\psi_1^\mu, n_\mu = 0\right\rangle, \\ |1\rangle_\mu &\equiv \hat{a}_\mu^\dagger |\emptyset\rangle = \left|\psi_0^\mu, n_\mu = 1\right\rangle, \end{aligned} \tag{1}$$

where $\hat{a}_\mu^\dagger$ is the photon creation operator and $|\emptyset\rangle = |\psi_0, n_\mu = 0\rangle$ is the vacuum state. Thus, the logical state of the qubit depends on whether the excitation is stored within the spin ensemble or in the quantized electromagnetic field of the resonator.

B. Setup and system Hamiltonian

In this section, we describe the elementary unit of the scalable setup used to implement the quantum gates, i.e., a system of two qubits ($\mu = \mathcal{A}, \mathcal{A}'$). These consist of two distinct SEs, coupled to the modes of two different resonators, as shown in Fig. 1. The extension of the scheme to a bipartite linear lattice of cavities is straightforward [28]. The two SEs are formed by effective $s = 1/2$ spins, with different energy gaps: ω^A is close to the harmonic ω_c^A of the cavity belonging to qubit $\mathcal{A}$, and $\omega^{A'}$ is close to the harmonic $\omega_c^{A'}$ of the cavity of $\mathcal{A}'$ (see Fig. 2). A third unit $\mathcal{B}$, interposed between the qubits $\mathcal{A}$ and $\mathcal{A}'$, includes a resonator coupled to a nonlinear element, such as a transmon or a Cooper-pair box, which is exploited to implement the CZ. In the following, we shall refer to this nonlinear element as the CPB, and we will consider it as a three-level system [29]. We stress that the CPB is not used to encode the qubits and is left in its ground state always except during the implementation of the two-qubit gates. In

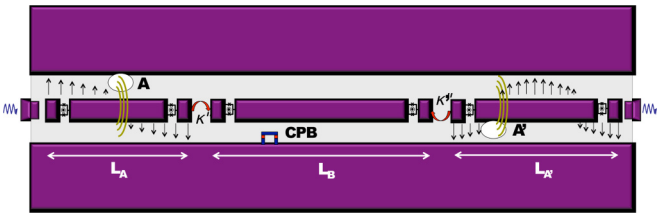

FIG. 1. (Color online) Sketch of the elementary unit of the scalable setup. Black arrows indicate the electric field distribution of different harmonics in each resonator. Qubits $\mathcal{A}$ and $\mathcal{A}'$ include each an ensemble of $s = 1/2$ spins, placed at the antinodes of the magnetic field (rotational lines) of the respective cavity modes. These are coupled to each other through the auxiliary unit $\mathcal{B}$, formed by a resonator and a superconducting nonlinear element (a CPB).

the cavity of $\mathcal{B}$ we consider two different harmonics ω_c^B and $\omega_c^{B'}$, respectively close to the gaps Ω^B and $\Omega^{B'}$ of the CPB.

The total Hamiltonian of the SEs and CPB, coupled to the cavity modes, is given by

$$\hat{H} = \hat{H}_{spin} + \hat{H}_{CPB} + \hat{H}_{ph} + \hat{H}_{int} + \hat{H}_{ph\text{-}ph}. \tag{2}$$

The first term describes the SEs of the qubits $\mathcal{A}$ and $\mathcal{A}'$ as independent harmonic oscillators [30] ($\hbar \equiv 1$):

$$\hat{H}_{spin} = \omega^A \hat{b}_A^\dagger \hat{b}_A + \omega^{A'} \hat{b}_{A'}^\dagger \hat{b}_{A'}. \tag{3}$$

The CPB is treated as an effective three-level system [31]:

$$\hat{H}_{CPB} = \Omega^B \left|\psi_1^B\right\rangle\left\langle\psi_1^B\right| + (\Omega^{B'} + \Omega^B)\left|\psi_2^B\right\rangle\left\langle\psi_2^B\right|. \tag{4}$$

The time-dependent photonic term is entirely responsible for the manipulation of the qubits. It can be expressed as

$$\hat{H}_{ph} = \sum_{\gamma = A, A', B, B'} \omega_c^\gamma(t) \hat{a}_\gamma^\dagger \hat{a}_\gamma, \tag{5}$$

where $\omega_c^\gamma(t) = \omega_c^\gamma(0) + \Delta_c^\gamma(t)$. Hereafter, we will use the interaction picture, with $\hat{H}_0 = \hat{H}_{spin} + \hat{H}_{CPB} + \hat{H}_{ph}(t = 0)$. Hence, within the rotating-wave approximation the spin-photon and CPB-photon coupling Hamiltonians take the

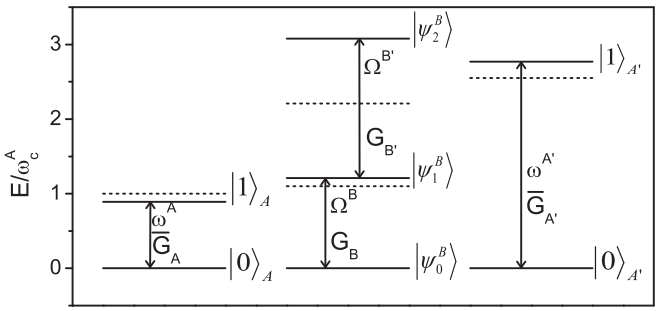

FIG. 2. Level diagram (solid lines) of the two $s = 1/2$ spin ensembles, used to define the qubits, and of the interposed CPB, which is employed to implement the two-qubit CZ gate. The spin-photon coupling strengths are indicated as $\bar{G}_\gamma$ and correspond to transitions of frequency ω^γ between the spin-ensemble states $|\psi_0^\gamma\rangle$ and $|\psi_1^\gamma\rangle$ ($\gamma = A, A'$). The CPB-cavity couplings are indicated by G_γ. Dashed lines represent the frequencies of the photonic modes inside each cavity.

form:

$$\hat{H}_{int} = G_B\left[\hat{a}_B^\dagger \left|\psi_0^B\right\rangle\!\left\langle\psi_1^B\right| e^{i(\omega_c^B-\Omega^B)t} + \text{H.c.}\right] + G_{B'}\left[\hat{a}_{B'}^\dagger \left|\psi_1^B\right\rangle\!\left\langle\psi_2^B\right| e^{i(\omega_c^{B'}-\Omega^{B'})t} + \text{H.c.}\right] + \sum_{\gamma=A,A'} \bar{G}_\gamma\left[\hat{a}_\gamma^\dagger \hat{b}_\gamma e^{i(\omega_c^\gamma-\omega^\gamma)t} + \text{H.c.}\right]. \quad (6)$$

Here, the coupling constants $\bar{G}_\gamma$ are enhanced by a factor $\sqrt{N}$ with respect to their single-spin counterparts (see, e.g., Ref. [15] for a detailed derivation).

Finally, the last term in Eq. (2) describes the photon-hopping processes induced by the capacitive coupling between the modes A and B (A' and B') of the neighboring cavities [33,34]:

$$\hat{H}_{ph\text{-}ph} = -\kappa \hat{a}_A^\dagger \hat{a}_B e^{i(\omega_c^A-\omega_c^B)t} - \kappa' \hat{a}_{A'}^\dagger \hat{a}_{B'} e^{i(\omega_c^{A'}-\omega_c^{B'})t} + \text{H.c.} \quad (7)$$

By properly engineering the two different cavities, the coupling between other modes can be easily made negligible.

C. Description of the quantum gates

Resonant processes involving the absorption (emission) of the photons entering the hybrid encoding in Eq. (1) are exploited to perform one- and two-qubit gates. These processes are induced by "shift pulses," in which the cavity frequency is varied by a quantity Δ_c^γ for a suitable amount of time. Experimentally, the resonator frequencies have already been shown to be variable up to tenths of the fundamental-mode frequency [24], even on a nanosecond time scale [25,30]. In order to make the manipulation experimentally easier, we choose $\omega_c^B(0)$ to be intermediate between $\omega_c^A(0)$ and Ω^B, while $\omega_c^{A'}(0)$ is close to $\omega_c^{B'}(0)$, and $\omega_c^{B'}(0)$ is close to $\Omega^{B'}$ (see Fig. 2).

Single-qubit rotations. In the idle mode $\Delta_c^\gamma(t) = 0$, the photon frequencies are largely detuned from the spin energy gaps [$|\omega_c^\gamma(0) - \omega^\gamma| \gg \bar{G}_\gamma$], and $\hat{H}_{int}$ is ineffective. In addition, the cavity modes A and A' are far-detuned from B and B' ($|\omega_c^A - \omega_c^B| \gg \kappa, |\omega_c^{A'} - \omega_c^{B'}| \gg \kappa'$), and the effect of $\hat{H}_{ph\text{-}ph}$ is negligible. Single-qubit gates can thus be performed independently on each qubit.

In particular, off-resonance pulses are employed to obtain a rotation by an arbitrary angle about the z axis of the Bloch sphere. These induce a phase difference between the $|0\rangle_\mu$ and $|1\rangle_\mu$ states of the hybrid qubits [Eq. (1)]. We assume for simplicity steplike pulses $\Delta_c^\gamma(t) \equiv \delta_c^\gamma\,\theta(\tau/2 - |t - t_0 - \tau/2|)$, so that a generic phase shift $\hat{R}_\varphi$ is performed, with $\varphi = -\delta_c^\gamma \tau$. In the basis $\{|0\rangle_\mu, |1\rangle_\mu\}$, this rotation takes the form

$$\hat{R}_\varphi = \begin{pmatrix} 1 & 0 \\ 0 & e^{-i\delta_c^\gamma \tau} \end{pmatrix}. \quad (8)$$

This coincides with a rotation around the z axis up to an overall phase, where $\hat{R}_z(\varphi) = e^{-i\hat{\sigma}_z\varphi/2} = e^{-i\varphi/2}\hat{R}_\varphi$ and $\sigma_{\alpha=x,y,z}$ are the Pauli matrices. Conversely, rotations around the x axis,

$$\hat{R}_x(\varphi) = e^{-i\sigma_x\varphi/2} = \begin{pmatrix} \cos\frac{\varphi}{2} & -i\sin\frac{\varphi}{2} \\ -i\sin\frac{\varphi}{2} & \cos\frac{\varphi}{2} \end{pmatrix}, \quad (9)$$

are obtained by resonant processes in which the frequency of the cavity mode is tuned to match the corresponding energy gap of the SE [$\delta_c^\gamma = \omega^\gamma - \omega_c^\gamma(0)$, with $\gamma = A, A'$] for the proper amount of time, $\tau = \varphi/2\bar{G}_\gamma$ (see the Appendix for a more detailed analysis).

Controlled-Z gate. The CZ gate, which in the two-qubit basis $\{|0_\mathcal{A}0_{\mathcal{A}'}\rangle, |0_\mathcal{A}1_{\mathcal{A}'}\rangle, |1_\mathcal{A}0_{\mathcal{A}'}\rangle, |1_\mathcal{A}1_{\mathcal{A}'}\rangle\}$ is represented by the matrix

$$U_{CZ} = \begin{pmatrix} 1 & 0 & 0 & 0 \\ 0 & 1 & 0 & 0 \\ 0 & 0 & 1 & 0 \\ 0 & 0 & 0 & -1 \end{pmatrix}, \quad (10)$$

is implemented by means of a two-step Rabi oscillation of the CPB between $|\psi_0^B\rangle$ and $|\psi_2^B\rangle$. We describe here the CZ multistep pulse sequence, involving the auxiliary states

$$|\eta\rangle = |\emptyset\rangle \otimes \left|\psi_0^B, n_B = 1, n_{B'} = 1\right\rangle,$$
$$|\xi\rangle = |\emptyset\rangle \otimes \left|\psi_1^B, n_B = 0, n_{B'} = 1\right\rangle, \quad (11)$$
$$|\zeta\rangle = |\emptyset\rangle \otimes \left|\psi_2^B, n_B = 0, n_{B'} = 0\right\rangle,$$

where $|\emptyset\rangle = \otimes_{\mu=A,A'}|\psi_0^\mu, n_\mu = 0\rangle$ is the vacuum state of the two-qubit register. We schematically explain the effect of such a sequence on two qubits initialized in state $|1_\mathcal{A}1_{\mathcal{A}'}\rangle$:

(1) The first step corresponds to the hopping of the photons from the modes A and A' into the cavity modes B and B' of the unit $\mathcal{B}$, by means of two simultaneous π pulses that bring the two pairs of modes into resonance. This induces the transition $|1_\mathcal{A}1_{\mathcal{A}'}\rangle \longrightarrow |\eta\rangle$.

(2) As a second step, the photon of frequency ω_c^B is tuned to Ω^B by means of a π pulse, which transfers the excitation from the mode B to the intermediate level $|\psi_1^B\rangle$ of the CPB, carrying the system into the state $|\xi\rangle$.

(3) Then, a 2π pulse brings the mode of frequency $\omega_c^{B'}$ into resonance with $\Omega^{B'}$, thus inducing a complete Rabi flopping between the states $|\xi\rangle$ and $|\zeta\rangle$. In this process, a phase π is added to $|\xi\rangle$.

(4) Finally, the repetition of the first two steps brings the state back to $|1_\mathcal{A}1_{\mathcal{A}'}\rangle$, with an overall phase π. By properly setting the delay of the two π pulses corresponding to the previous steps (or by performing single-qubit phase shifts; see the Appendix), the associated absorption and emission processes yield a zero additional phase.

Conversely, the other basis states do not acquire any phase, as required for the CZ gate. In fact, the basis state $|0_\mathcal{A}1_{\mathcal{A}'}\rangle$ has only the high-energy photon which is driven to mode B', but is off resonance with the Ω^B gap, and hence is not absorbed. Instead, $|1_\mathcal{A}0_{\mathcal{A}'}\rangle$ contains only the low-energy photon, which is absorbed by the CPB, bringing it to the first excited state $|\psi_1^B\rangle$. However, the following Rabi flop does not occur, due to the absence of the higher-energy photon. Finally, the state $|0_\mathcal{A}0_{\mathcal{A}'}\rangle$ is completely unaffected by the pulse sequence, because of the absence of both photons.

III. EFFECT OF DECOHERENCE

The interaction of the system with the environment tends to introduce errors in the implemented quantum gates. Hereafter, we introduce the theoretical approach that will be employed

to simulate the dynamics in an open-system scenario, in order to assess the robustness of the present scheme with respect to the relevant decoherence sources.

A. Master-equation approach

The time evolution of the system density matrix $\hat{\rho}$ is described within a Markovian approximation and a Lindblad-type dynamics, with the Liouville–von Neumann equation of motion [35]:

$$\frac{d}{dt}\hat{\rho} = -i[\hat{H},\hat{\rho}] + \sum_j \Gamma_j \mathcal{L}_{\hat{x}_j}[\hat{\rho}] + \sum_j \gamma_j \mathcal{L}_{\hat{x}_j^\dagger \hat{x}_j}[\hat{\rho}], \quad (12)$$

where Γ_j and γ_j are respectively the damping and pure-dephasing rates of the field $\hat{x}_j$. The Lindblad term for an arbitrary operator $\hat{x}$ is given by

$$\mathcal{L}_{\hat{x}}[\hat{\rho}] = -\tfrac{1}{2}(\hat{x}^\dagger \hat{x}\hat{\rho} + \hat{\rho}\hat{x}^\dagger \hat{x}) + \hat{x}\hat{\rho}\hat{x}^\dagger. \quad (13)$$

The density matrix approach followed in the present work allows us to include the effects of relaxation and pure dephasing on each element involved in the scheme. If the operator $\hat{x}_j$ destroys an excitation in the system, terms like $\mathcal{L}_{\hat{x}_j}[\hat{\rho}]$ account for energy losses, while pure dephasing processes are described by $\mathcal{L}_{\hat{x}_j^\dagger \hat{x}_j}[\hat{\rho}]$. We note that the former provide the most important contribution for photons [36] (with $\hat{x}_j = \hat{a}_j$, $j = A, A', B, B'$), while the latter are dominant for the CPB [31] ($\hat{x}_j = |\psi_j^B\rangle\langle\psi_{j+1}^B|$, $j = 0,1$). Hence, we initially study the fidelity of the quantum gates as a function of the photon leakage rate and the CPB pure-dephasing rate. We then include two further sources of error. The first one is represented by energy loss from the superconducting nonlinear element, which however is not expected to appreciably alter the gate fidelity, since the loss rate is usually smaller than the pure-dephasing rate. The second one is given by the pure dephasing of the spin ensemble, whose effect on the system dynamics is similarly small.

For the simulations, we represent each field as a matrix in the Fock-state basis, and truncate it at a number of total excitations previously checked for convergence. The total Hamiltonian, Eq. (2), and the density matrix master equation of the whole system, Eq. (12), are built from tensor products of these operators. Then, the equation of motion for $\hat{\rho}$ is numerically integrated, in the interaction picture, by using a standard Runge-Kutta approximation.

B. Numerical results

In order to investigate the effects of decoherence on quantum-information processing, the numerical simulation of single- and two-qubit gates reported in Ref. [22] has been reproduced by using the master-equation formalism outlined above. As in Ref. [22], we identify the modes A and A' (B and B') with the first and second (second and third) harmonics of the respective cavities (see also the sketch in Fig. 1), and assume the following values for the fundamental cavity frequencies: $\omega_c^0/2\pi = 22$, 21, 12.5 GHz for the units $\mathcal{A}$, $\mathcal{A}'$, $\mathcal{B}$, respectively. With these choices, photon hopping between modes other than those included in Eq. (7) is negligible. We also assume realistic values of the CPB-cavity ($G_\gamma/2\pi = 30$–45 MHz) and SE-cavity ($\bar{G}_\gamma/2\pi = 30$ MHz) coupling rates, with the latter corresponding to $N \sim 10^{12}$ spins 1/2 (see Ref. [19]). Finally, the photon-tunneling rate is $\kappa = \kappa' = 2\pi \times 25$ MHz, which has already been shown experimentally [33].

Since the time required to implement the two-qubit CZ gate is much longer than that corresponding to the single-qubit rotations, this gate is more error prone. Therefore, we consider the CZ gate as a test bed for the robustness of our quantum-information processing scheme. As a figure of merit for the CZ gate, we compute its fidelity $\mathcal{F}$:

$$\mathcal{F} = \sqrt{\langle\psi|\hat{\rho}|\psi\rangle}, \quad (14)$$

where $\hat{\rho}$ is the final density matrix and $|\psi\rangle$ the target state.

First, we investigate the effects of photon leakage and pure dephasing of the CPB, described by the last two terms in Eq. (12). For each cavity mode, we have assumed a photon-leakage rate that is proportional to the relative mode frequency $\Gamma_i = \omega_c^i/Q$, while the quality factor is the same for all the relevant cavity modes [23]. Furthermore, we notice that the same dephasing rate has also been assumed for the two Lindblad operators, $\hat{x}_j^\dagger \hat{x}_j = |\psi_{j+1}^B\rangle\langle\psi_{j+1}^B|$ ($j = 0,1$), acting on the two relevant CPB transitions, without loss of generality. Figure 3(a) reports the fidelity as a function of the resonator quality

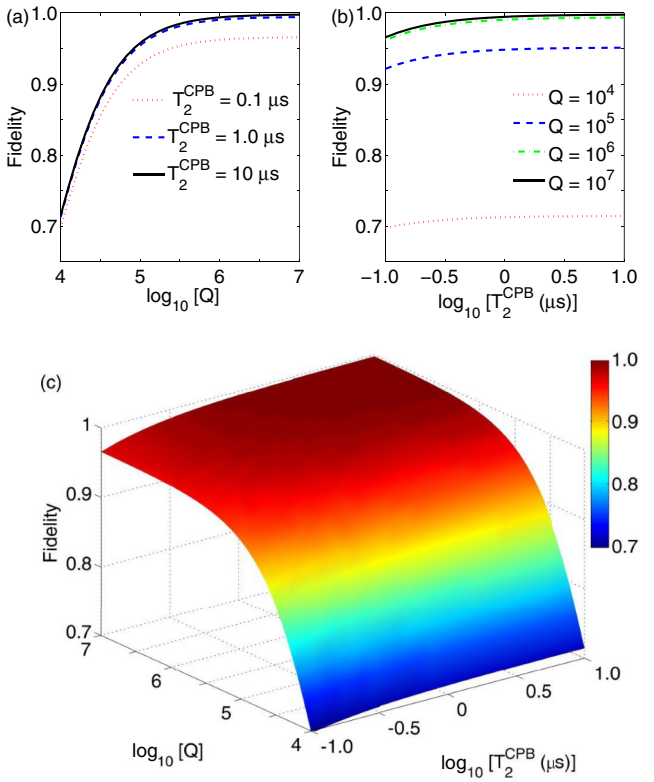

FIG. 3. (Color online) Fidelity of the CZ gate as a function of the quality factor Q of the resonators, for different values of the CPB dephasing time T_2^{CPB} (a) and of the CPB dephasing time T_2^{CPB}, for different values of the quality factor Q (b). The system is initialized in the superposition of the computational basis states $(|0_\mathcal{A} 0_{\mathcal{A}'}\rangle + |1_\mathcal{A} 1_{\mathcal{A}'}\rangle)/\sqrt{2}$. (c) Two-dimensional surface of $\mathcal{F}(Q, T_2^{CPB})$. Both Q and T_2^{CPB} are varied in a realistic range, which can be reached with available technology. The gate fidelity is represented both by the colors and by the height of the surface.

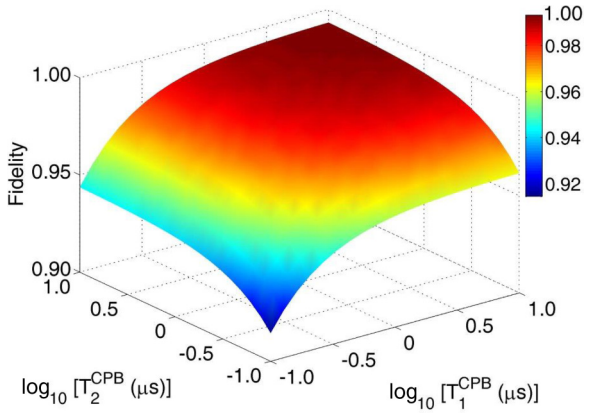

FIG. 4. (Color online) CZ-gate fidelity as a function of T_1^{CPB} and T_2^{CPB}, assuming $Q = 10^6$. The calculated fidelity is represented both by the colors and by the height of the surface.

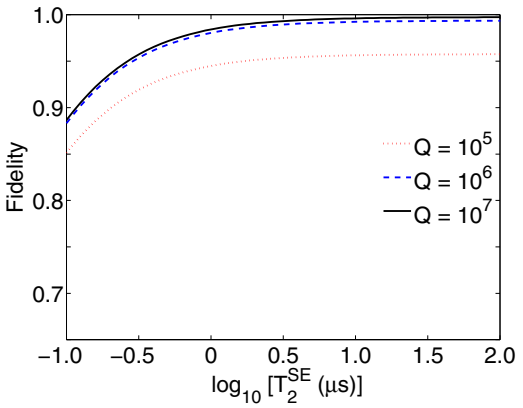

FIG. 5. (Color online) Fidelity of the CZ gate as a function of the spin-ensemble dephasing time $T_2^{SE} = 1/\gamma_{SE}$. The three curves refer to different Q factors and are calculated assuming $T_2^{CPB} = 10\ \mu s$.

factor Q. Different curves refer to different values of the CPB dephasing time $T_2^{CPB} = 1/\gamma_{CPB}$, chosen in a realistic range. In particular, the lower bound of $T_2^{CPB} = 0.1\ \mu$s is typical of charge qubits, in the regime $E_C \geqslant E_J$ [17]. Dephasing times of the order of $T_2^{CPB} = 10\ \mu$s have already been demonstrated experimentally [32] for CPBs in the transmonic regime $E_J \approx 10E_C$, which is close to the range of parameters we are exploring [31]. With such values of T_2^{CPB} and with Q approaching 10^6, we obtain a fidelity above 99%. In Fig. 3(b) the fidelity is plotted as a function of T_2^{CPB}, for different values of Q. The dependence of the fidelity on T_2^{CPB} is much weaker than that on Q. This results from the fact that the excited states of the CPB are populated only for a fraction of the total gating time. Figure 3(c) reports the overall dependence of the CZ-gate fidelity on the cavity quality factor and on the CPB dephasing time. For the simulation reported in Fig. 3, the system is initialized in a superposition state $(|0_A 0_{A'}\rangle + |1_A 1_{A'}\rangle)/\sqrt{2}$. This state is one of the most error prone, as it introduces in the calculation the relative phase between $|1_A 1_{A'}\rangle$ (in which both qubits are subject to damping and dephasing) and $|0_A 0_{A'}\rangle$, which is completely unaffected by the pulse sequence. Consequently, other superposition states lead to similar or slightly larger fidelities.

Typically, T_1^{CPB} is larger than T_2^{CPB} in CPBs [31]. In any case, we have checked that the inclusion of a relaxation term for the CPB does not reduce the gate fidelity appreciably. A color map of the CZ-gate fidelity as a function of T_1^{CPB} and T_2^{CPB} is reported in Fig. 4. We note a slightly more pronounced dependence of $\mathcal{F}$ on the relaxation time T_1^{CPB} than on the dephasing time T_2^{CPB}. However, in the regime [31] examined here we can assume $T_2^{CPB} \approx 10\,\mu s$ and $T_1^{CPB} > T_2^{CPB}$, leading (in a cavity with $Q = 10^6$) to values of $\mathcal{F}$ above 99%.

As far as photons are concerned, it has been experimentally shown that pure dephasing of the cavity modes is practically negligible (see, e.g., Ref. [36], where the measured value of the dephasing time T_2^{ph} approximately corresponds to twice the value of the photon decay time T_1^{ph}). Finally, we have included in the equation of motion a pure-dephasing term acting on the spin ensembles. The calculated fidelity at the end of a CZ gate is plotted in Fig. 5 as a function of the spin-ensemble dephasing time T_2^{SE}, for different values of Q. We note that for $T_2^{SE} > 1\ \mu$s, the fidelity of a single gate (which takes about 50 ns) is nearly independent of T_2^{SE}, whereas the dependence on Q is much more pronounced. In that limit, the spin-dephasing rate does not appreciably affect the system dynamics.

IV. PROOF-OF-PRINCIPLE EXPERIMENT

We describe here a simpler, not scalable setup, which could be exploited for the first proof-of-principle demonstrations of the present scheme. This setup includes a single cavity, coupled to a CPB and an ensemble of equally oriented $s = 1$ spins, as schematically shown in Fig. 6 [37]. We refer here not to disordered diluted systems, but to crystals of equally oriented magnetic ions diluted in a nonmagnetic matrix (see, e.g., Ref. [38]). In the low-excitation regime, the spin ensemble can be modeled by two independent harmonic oscillators, related to two different magnetic-dipole transitions from the $m = 0$ ground state of the single spin, namely, those to the $m = -1$ and $m = 1$ states. This can be achieved by properly choosing a system with easy-plane magnetic anisotropy, which provides a zero-field splitting between the $m = 0$ ground state and the excited $m = \pm 1$ doublet, and in the presence of a small static magnetic field. The corresponding creation operators (excitation energies) are given by $\hat{b}_A^\dagger = \frac{1}{\sqrt{N}} \sum_{q=1}^N |-1\rangle\langle 0|_q$ and $\hat{b}_{A'}^\dagger = \frac{1}{\sqrt{N}} \sum_{q=1}^N |1\rangle\langle 0|_q$ (ω^A and $\omega^{A'}$), while the ground state of the SE is $|\psi_0\rangle = |0_1 \cdots 0_N\rangle$. These spin modes,

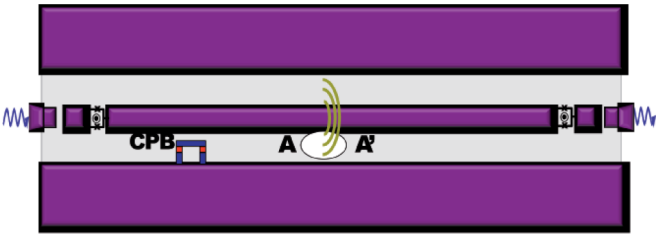

FIG. 6. (Color online) Sketch of the nonscalable setup for proof-of-principle experiments. Qubits $\mathcal{A}$ and $\mathcal{A}'$ are now encoded by using two different states of the same spin ensemble of $s = 1$ spins, coupled to two different harmonics of the same cavity.

together with the modes A and A' of the single cavity, allow us to introduce here a dual-rail encoding equivalent to that defined in Eq. (1) for the scalable architecture:

$$|0_{\mathcal{A}}0_{\mathcal{A}'}\rangle = \hat{b}^{\dagger}_{A}\hat{b}^{\dagger}_{A'}|\emptyset\rangle, \quad |0_{\mathcal{A}}1_{\mathcal{A}'}\rangle = \hat{b}^{\dagger}_{A}\hat{a}^{\dagger}_{A'}|\emptyset\rangle,$$
$$|1_{\mathcal{A}}0_{\mathcal{A}'}\rangle = \hat{a}^{\dagger}_{A}\hat{b}^{\dagger}_{A'}|\emptyset\rangle, \quad |1_{\mathcal{A}}1_{\mathcal{A}'}\rangle = \hat{a}^{\dagger}_{A}\hat{a}^{\dagger}_{A'}|\emptyset\rangle, \tag{15}$$

where $|\emptyset\rangle = |\psi_0, n_A = 0, n_{A'} = 0\rangle$. For the qubit manipulation, and specifically for the two-qubit gate, we exploit the lowest three levels of the CPB ($|\psi_0^B\rangle$, $|\psi_1^B\rangle$, and $|\psi_2^B\rangle$), with transition energies Ω^B and $\Omega^{B'}$, as in the scalable scheme. In addition, the two harmonics of the resonator that are taken into account have frequencies ω_c^A and $\omega_c^{A'}$: ω_c^A is intermediate between ω^A and Ω^B, while $\omega_c^{A'}$ is intermediate between $\omega^{A'}$ and $\Omega^{B'}$. In this way, the cavity mode ω_c^A ($\omega_c^{A'}$) can be coupled both to the spin gap ω^A ($\omega^{A'}$) and to the superconducting gap Ω^B ($\Omega^{B'}$). As in the scalable setup, the CPB does not enter the definition of the qubits, for it remains in its ground state in all the computational space.

Single-qubit rotations are implemented in a way similar to that described for the scalable setup: rotations about the z axis of the Bloch sphere, $\hat{R}_z(\varphi)$, are realized by means of off-resonant pulses, while $\hat{R}_x(\varphi)$ are performed by tuning ω_c^{γ} to ω^{γ} for the proper amount of time ($\gamma = A, A'$). However, as the photons that are involved in the encoding of the two qubits correspond to different harmonics of the same cavity, the $\hat{R}_z(\varphi)$ rotations applied to qubits A and A' are not independent. Indeed, by applying a pulse of amplitude $2\delta_c$ to the second harmonic for a time τ, one also varies the phase of the third harmonic by an amount of $3\delta_c\tau$. In the two-qubit basis, we thus obtain the transformation

$$\hat{R}_{zz}(\tau) = \begin{pmatrix} 1 & 0 & 0 & 0 \\ 0 & e^{-2i\delta_c\tau} & 0 & 0 \\ 0 & 0 & e^{-3i\delta_c\tau} & 0 \\ 0 & 0 & 0 & e^{-5i\delta_c\tau} \end{pmatrix}. \tag{16}$$

A rotation of, e.g., the first qubit can however be performed without affecting the second one, by exploiting the equality

$$\hat{R}_{zz}(\tau)[\hat{R}_x(\varphi)\otimes\hat{I}]\hat{R}_{zz}(\tau) = \hat{R}_y(\varphi)\otimes\hat{I}, \tag{17}$$

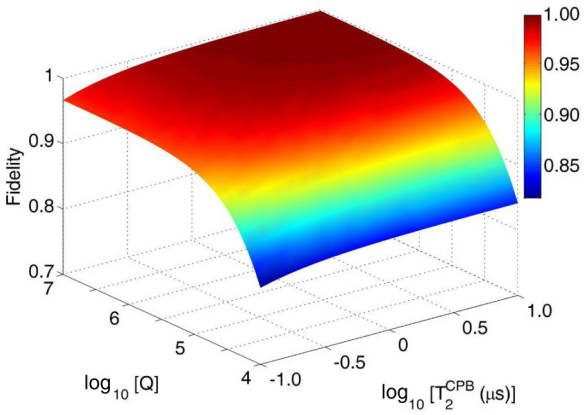

FIG. 7. (Color online) Fidelity of the CZ gate as a function of Q and T_2^{CPB} in the nonscalable setup. The calculated fidelity is represented both by the colors and by the height of the surface.

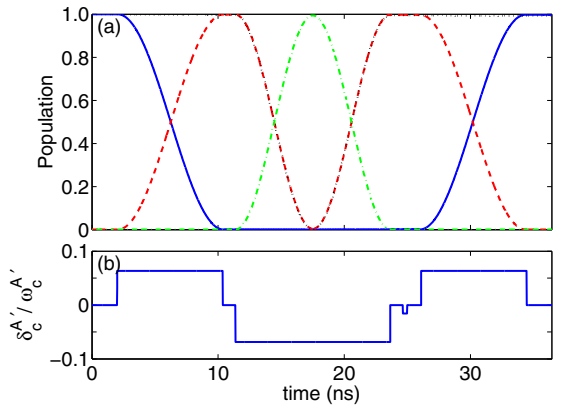

FIG. 8. (Color online) (a) Population of the fields as a function of time during a CZ gate, with the system initialized in state $|1_{\mathcal{A}}1_{\mathcal{A}'}\rangle$. The continuous, dashed, dot-dashed, and dotted lines represent the time dependences of $\langle\hat{a}^{\dagger}_A\hat{a}_A\rangle$, $\langle|\psi_1^B\rangle\langle\psi_1^B|\rangle$, $\langle|\psi_2^B\rangle\langle\psi_2^B|\rangle$, and $\langle\hat{a}^{\dagger}_{A'}\hat{a}_{A'}\rangle$, respectively. (b) Pulse sequence representing the relative frequency variations of the cavity during the implementation of the CZ in the nonscalable setup.

which holds for $\tau = 3\pi/2\delta_c$ [39]. In this way, we demonstrate the ability to implement independent $\hat{R}_y$ rotations on each qubit. This, together with rotations about the x axis, allows us to obtain any single-qubit gate.

The CZ gate can be implemented as in the scalable setup. Here, however, a single resonator is involved, and no photon hopping is needed: this reduces the overall time required to implement the quantum gate. Figure 7 is a color map of the fidelity in a CZ gate, as a function of the two parameters accounting for the two included sources of error: the resonator quality factor Q, accounting for photon leakage, and the CPB dephasing time T_2^{CPB}. The plot is similar to that of Fig. 3: the larger Q and T_2^{CPB}, the larger the fidelity. However, as the implementation of a single CZ gate here is faster, the photon leakage is less relevant: slightly larger values of the fidelity correspond to the same values of Q. In Fig. 8(a) we plot the expectation value of the number operators as a function of time, i.e., $\langle\hat{a}^{\dagger}_A\hat{a}_A\rangle_t = \mathrm{Tr}[\hat{\rho}(t)\hat{a}^{\dagger}_A\hat{a}_A]$, and analogously for the other fields. The parameters corresponding to photon loss and pure dephasing of the CPB are given by $Q = 10^6$ and $T_2^{CPB} = 10\ \mu$s. The system is initialized in state $|1_{\mathcal{A}}1_{\mathcal{A}'}\rangle$. Figure 8(b) displays the profile of the steplike pulse sequence employed in the simulation: The first π pulse brings the photon of frequency ω_c^A into resonance with the CPB gap Ω^B, leading to the absorption of the photon A. The second one is a 2π pulse, which induces a full Rabi flop between states $|\psi_1^B\rangle$ and $|\psi_2^B\rangle$. Then an off-resonant pulse is used to implement a rotation about the z axis which corrects the unwanted phase acquired during the Rabi oscillation. Finally, a π pulse brings the system to state $-|1_{\mathcal{A}}1_{\mathcal{A}'}\rangle$, while the other basis states are unaffected.

V. DISCUSSION

In the present section, we briefly discuss the possible consequences of the above decoherence mechanisms for quantum-information processing. In addition, we discuss the physical implementation of the qubit, and specifically of the component represented by the spin ensemble.

A. Errors resulting from the decoherence mechanisms

The results reported in the previous sections show that the main source of error in our scheme is represented by photon loss. Conversely, since the CPB is excited only during part of the implementation of the CZ gate, $T_2^{CPB} > 1\ \mu$s is sufficient to guarantee a high fidelity of the gates. Quality factors somewhat smaller than 10^5 already lead to fidelity values $\mathcal{F} > 0.90$–0.95, but it could be realistic to assume $Q \approx 10^6$–10^7, as shown in Ref. [21]. In the limit of $Q = 10^8$, the photon lifetime would reach 0.3 ms, very close to the coherence time of the best SEs. Within this time scale, several quantum gates could be performed on the proposed setup, leading to the implementation of complex quantum algorithms, as well as the simulation of different quantum systems [40]. Other decoherence sources, such as relaxation of the CPB, are found to be ineffective, in a realistic range of parameters.

The fact that the dominant source of error is given by photon loss represents a potential advantage for the implementation of quantum computation [41]. In fact, within the dual-rail encoding we propose, the photon loss corresponds to a locatable error, and can in principle be detected without requiring any redundant multiqubit encoding [42]. We note that the same effect is produced by inhomogeneous broadening of the spin ensemble, which can induce the leakage of the subsystem state out of the computational space. In fact, in the presence of inhomogeneities, the state $|\psi_1^{\mu}\rangle$ decays into other collective modes of the spin ensemble, which are decoupled from the cavity mode (see the discussion in Sec. VB). Therefore, neither photon loss nor inhomogeneous broadening of the SE induces an undesired bit flip or phase shift. These can only result from imperfections in the pulses that are used for the quantum-gate implementation. In one-way quantum computing [43], the presence of only locatable errors was shown to result in a significant increase of the error rate that is compatible with fault-tolerant quantum computation [44].

B. Physical implementation of the spin ensemble

In single spins, the dephasing time can reach the value of 0.1–1 ms [38]. As stated above, an additional source of decoherence in SEs is represented by inhomogeneous broadening [45,46]. This is essentially due to the presence of disorder, which spreads the emitter's bare frequencies and spin-photon couplings within the ensemble. In the spin-wave representation, the effect of such disorder is the dynamical coupling of the super-radiant ($k = 0$) mode with the subradiant ($k \neq 0$) ones. Here k is a quantum number labeling the one-boson states (and it coincides with the wave vector of the magnons in a translationally invariant arrangement of the spins). A transition to these subradiant modes can be regarded as an irreversible population leakage out of the subspace $\{|\psi_0\rangle,|\psi_1\rangle\}$, and thus of the computational space. In the absence of cavity-spin coupling, this leakage effect depends crucially on the width Δ of the distribution in the emitter's bare frequencies $\rho(\omega)$, for the transition from $k = 0$ to the $k \neq 0$ modes takes place on a time scale $\tau \sim 1/\Delta$. However, a strong spin-cavity coupling provides a protection mechanism, by inducing an energy gap between the super-radiant and the subradiant modes [46]. If this gap is large enough, the system is efficiently protected from decoherence and the excitation can be stored in $|0\rangle_{\mu}$ for times much longer than $1/\Delta$. Indeed, out of resonance ($\delta_c^{\gamma} \gg \bar{G}_{\gamma}$) and in the presence of strong coupling ($\bar{G}_{\gamma} \gg \Delta$), the cavity has a dispersive effect that shifts the energy of the super-radiant mode by $\epsilon = -\bar{G}_{\gamma}^2/\delta_c^{\gamma}$. Provided that $\epsilon \gg \Delta$ and that the tail of the emitter's bare frequency distribution $\rho(\omega)$ falls off sufficiently fast (as in the case of a Gaussian profile) [45], the super-radiant mode is energetically separated from the subradiant modes and the cavity protects the information stored in the spin ensemble.

Hence, the robustness of the scheme relies on the choice of a suitable spin system. In order to reduce the effect of inhomogeneous broadening, we need an ordered system, or a spin system with Gaussian broadening, possibly isotropic and diluted in a nonmagnetic matrix to avoid dipolar interactions, which typically lead to Lorentzian line shapes. Another important mechanism of decoherence is represented by hyperfine interactions between electronic and nuclear spins. These tend to reduce the intrinsic decoherence time of the individual spins, and introduce a Gaussian broadening of the transition energies. At least the largest contribution to the hyperfine couplings, represented by the contact term, can be avoided by considering spin systems where the magnetic ions have nonmagnetic nuclei.

A class of spin systems that provides interesting and yet unexplored possibilities in this respect is represented by molecular nanomagnets [47]. For example, high-spin molecules possess magnetic-dipole transitions (e.g., those between the states $|m = 0\rangle$ and $|m = \pm 1\rangle$) whose amplitude is roughly proportional to the spin length. This, along with the possible localization of the molecules in the nanometer-sized constrictions of the resonator, enabled by efficient deposition techniques, might allow one to achieve the strong-coupling regime even with a single molecule [48]. Such an achievement would eliminate the contribution to decoherence resulting from inhomogeneous broadening. In this way the only relevant source of error of the spins is given by pure dephasing of the single molecule (see Fig. 5), whose coherence time can reach values of several microseconds [49]. A further opportunity is represented by the suppression of the intrinsic decoherence time of the spins. This could in principle be achieved by exploiting protected degrees of freedom within the molecular spin cluster, such as spin chirality [50].

VI. CONCLUSIONS

In conclusion, we have studied the robustness of the quantum gates realized with a recently proposed hybrid spin-photon qubit encoding, in which both photonic and spin degrees of freedom enter on an equal footing in the definition of the qubits. This allows one to implement all the required quantum gates by a unique means, namely, by tuning the resonator frequencies through shift pulses, and to limit the role played by nonlinear superconducting elements, such as Cooper-pair boxes.

In such a scheme, the main decoherence processes are represented by photon loss and pure dephasing of the superconducting elements. The simulation of these effects within a master-equation formalism allowed us to test the robustness of our scheme, and to compute the fidelity of single- and two-qubit gates in a realistic range of parameters. We find

that photon leakage is the most relevant source of error, while pure dephasing only slightly alters the gate fidelity. Reasonable values of the resonator quality factor ($Q \approx 10^5$) lead to high values of the gate fidelity ($\mathcal{F} > 0.95$) for a single gate. Moreover, photon losses lead to population leakage out of the computational space, and can thus be detected without requiring any redundant multiqubit encoding. Since the Cooper-pair box is involved only as an auxiliary unit during the implementation of two-qubit gates, the computation is weakly affected by its possibly short decoherence times.

ACKNOWLEDGMENTS

This work was financially supported by the Italian FIRB Project No. RBFR12RPD1 of the Italian MIUR "New Challenges in Molecular Nanomagnetism: From Spin Dynamics to Quantum-Information Processing."

APPENDIX: RESONANT EVOLUTION

In this appendix, we determine the time evolution of qubit μ in the resonant regime. We start from the following Hamiltonian:

$$\hat{H} = \omega^{\mu}\hat{b}_{\mu}^{\dagger}\hat{b}_{\mu} + \omega_c^{\mu}\hat{a}_{\mu}^{\dagger}\hat{a}_{\mu} + \bar{G}_{\mu}\left[\hat{a}_{\mu}^{\dagger}\hat{b}_{\mu}e^{i(\omega_c^{\mu}-\omega^{\mu})t} + \hat{a}_{\mu}\hat{b}_{\mu}^{\dagger}e^{-i(\omega_c^{\mu}-\omega^{\mu})t}\right], \quad \text{(A1)}$$

in which we take into account only the relevant interactions involving qubit μ. In the limit of large detuning between cavity μ and cavity B, photon-hopping terms are ineffective. Then we set $\delta_c^{\mu} = \omega^{\mu} - \omega_c^{\mu}$ and we determine analytically the time evolution of a state initialized (in the interaction picture) in a general superposition $\alpha|0\rangle_{\mu} + \beta|1\rangle_{\mu}$ of the single-qubit basis. At $t = 0$ the cavity is far detuned ($\delta_c^{\mu} \gg \bar{G}_{\mu}$) from the spin gap and the resonance condition $\omega^{\mu} = \omega_c^{\mu}$ is established at $t = t_0$. As the Hamiltonian conserves the total number N_{ex} of excitations, we can reduce it to the subspace $N_{ex} = 1$, where

$$\hat{H} = \begin{pmatrix} \omega^{\mu} & \bar{G}_{\mu} \\ \bar{G}_{\mu} & \omega^{\mu} \end{pmatrix}. \quad \text{(A2)}$$

The single-qubit evolution (in the interaction picture) can be summarized by the following unitary operator:

$$U_1 = \begin{pmatrix} \cos(\bar{G}_{\gamma}\tau) & -ie^{-i\delta_c^{\gamma}t}\sin(\bar{G}_{\gamma}\tau) \\ -ie^{i\delta_c^{\gamma}t_0}\sin(\bar{G}_{\gamma}\tau) & e^{-i\delta_c^{\gamma}(t-t_0)}\cos(\bar{G}_{\gamma}\tau) \end{pmatrix} \quad \text{(A3)}$$

where $\tau = t - t_0$. By comparing Eqs. (9) and (A3), we note that the additional phase $\varphi = -\delta_c^{\gamma}\tau$ of the $|1\rangle_{\mu}$ qubit state is straightforwardly corrected by an $\hat{R}_{-\varphi}$ rotation. Furthermore, in order to obtain a rotation about the x axis of the Bloch sphere, we need to choose t_0 as an integer multiple of $2\pi/\delta_c^{\gamma}$. This auxiliary degree of freedom can be exploited to obtain a rotation about an arbitrary axis in the xy plane. In fact, by applying $\hat{R}_{-\varphi}$ and then U_1, we obtain the unitary operator:

$$U_2 = \begin{pmatrix} \cos(\bar{G}_{\gamma}\tau) & -ie^{-i\delta_c^{\gamma}t_0}\sin(\bar{G}_{\gamma}\tau) \\ -ie^{i\delta_c^{\gamma}t_0}\sin(\bar{G}_{\gamma}\tau) & \cos(\bar{G}_{\gamma}\tau) \end{pmatrix}, \quad \text{(A4)}$$

which has the form of a general rotation about an axis $\hat{n} = (n_x, n_y, 0)$, i.e., $\hat{R}_{\hat{n}}(\theta) = \cos\frac{\theta}{2} - i\sin\frac{\theta}{2}(n_x\sigma_x + n_y\sigma_y)$ [26], σ_{α} being the Pauli matrices. The same analysis holds also for two-qubit gates. Indeed, each pair of states involved in the resonant processes exploited to obtain the CZ gate evolves accordingly to Eq. (A3), with the only difference that in 2π processes the choice of t_0 is not relevant. In this way additional trivial phases acquired during 2π photon-hopping processes or during the second step of the evolution described in Sec. II C can be straightforwardly eliminated by short $\hat{R}_z$ operations as in the implementation of $\hat{R}_x$.

[1] Y. Makhlin, G. Schön, and A. Shnirman, Rev. Mod. Phys. **73**, 357 (2001).
[2] M. Devoret and J. M. Martinis, Quantum Inf. Process. **3**, 163 (2004).
[3] R. J. Schoelkopf and S. M. Girvin, Nature (London) **451**, 664 (2008).
[4] A. Wallraff, D. I. Schuster, A. Blais, L. Frunzio, R. S. Huang, J. Majer, S. Kumar, S. M. Girvin, and R. J. Schoelkopf, Nature (London) **431**, 162 (2004); H. Paik, D. I. Schuster, Lev S. Bishop, G. Kirchmair, G. Catelani, A. P. Sears, B. R. Johnson, M. J. Reagor, L. Frunzio, L. I. Glazman, S. M. Girvin, M. H. Devoret, and R. J. Schoelkopf, Phys. Rev. Lett. **107**, 240501 (2011).
[5] M. Hofheinz, E. M. Weig, M. Ansmann, R. C. Bialczak1, E. Lucero, M. Neeley, A. D. O'Connell, H. Wang, J. M. Martinis, and A. N. Cleland, Nature (London) **454**, 310 (2008); M. Mariantoni, H. Wang, R. C. Bialczak, M. Lenander, E. Lucero, M. Neeley, A. D. O'Connell, D. Sank, M. Weides, J. Wenner, T. Yamamoto, Y. Yin, J. Zhao, John M. Martinis, and A. N. Cleland, Nat. Phys. **7**, 287 (2011).
[6] G. Haack, F. Helmer, M. Mariantoni, F. Marquardt, and E. Solano, Phys. Rev. B **82**, 024514 (2010).
[7] F. Helmer, M. Mariantoni, A. G. Fowler, J. von Delft, E. Solano, and F. Marquardt, Europhys. Lett. **85**, 50007 (2009).
[8] J. Koch, T. M. Yu, J. Gambetta, A. A. Houck, D. I. Schuster, J. Majer, A. Blais, M. H. Devoret, S. M. Girvin, and R. J. Schoelkopf, Phys. Rev. A **76**, 042319 (2007).
[9] C. Rigetti, J. M. Gambetta, S. Poletto, B. L. T. Plourde, J. M. Chow, A. D. Córcoles, J. A. Smolin, S. T. Merkel, J. R. Rozen, G. A. Keefe, M. B. Rothwell, M. B. Ketchen, and M. Steffen, Phys. Rev. B **86**, 100506(R) (2012).
[10] Y. Ping, E. M. Gauger, and S. C. Benjamin, New J. Phys. **14**, 013030 (2012).
[11] Z.-L. Xiang, S. Ashhab, J. Q. You, and F. Nori, Rev. Mod. Phys. **85**, 623 (2013).
[12] P. Rabl, D. DeMille, J. M. Doyle, M. D. Lukin, R. J. Schoelkopf, and P. Zoller, Phys. Rev. Lett. **97**, 033003 (2006).
[13] A. Imamoglu, Phys. Rev. Lett. **102**, 083602 (2009).
[14] J. Verdu, H. Zoubi, Ch. Koller, J. Majer, H. Ritsch, and J. Schmiedmayer, Phys. Rev. Lett. **103**, 043603 (2009).
[15] J. H. Wesenberg, A. Ardavan, G. A. D. Briggs, J. J. L. Morton, R. J. Schoelkopf, D. I. Schuster, and K. Mølmer, Phys. Rev. Lett. **103**, 070502 (2009).

[16] J. Majer, J. M. Chow, J. M. Gambetta, Jens Koch, B. R. Johnson, J. A. Schreier, L. Frunzio, D. I. Schuster, A. A. Houck, A. Wallraff, A. Blais, M. H. Devoret, S. M. Girvin, and R. J. Schoelkopf, Nature (London) **449**, 443 (2007).
[17] J. Q. You and F. Nori, Phys. Today **58**(11), 42 (2005).
[18] M. Mariantoni, H. Wang, T. Yamamoto, M. Neeley, R. C. Bialczak, Y. Chen, M. Lenander, E. Lucero, A. D. O'Connell, D. Sank, M. Weides, J. Wenner, Y. Yin, J. Zhao, A. N. Korotkov, A. N. Cleland, and J. M. Martinis, Science **334**, 61 (2011).
[19] Y. Kubo, F. R. Ong, P. Bertet, D. Vion, V. Jacques, D. Zheng, A. Dréau, J.-F. Roch, A. Auffèves, F. Jelezko, J. Wrachtrup, M. F. Barthe, P. Bergonzo, and D. Esteve, Phys. Rev. Lett. **105**, 140502 (2010).
[20] D. I. Schuster, A. P. Sears, E. Ginossar, L. DiCarlo, L. Frunzio, J. J. L. Morton, H. Wu, G. A. D. Briggs, B. B. Buckley, D. D. Awschalom, and R. J. Schoelkopf, Phys. Rev. Lett. **105**, 140501 (2010).
[21] A. Megrant, C. Neill, R. Barends, B. Chiaro, Y. Chen, L. Feigl, J. Kelly, E. Lucero, M. Mariantoni, P. J. J. O'Malley, D. Sank, A. Vainsencher, J. Wenner, T. C. White, Y. Yin, J. Zhao, C. J. Palmstrom, J. M. Martinis, and A. N. Cleland, Appl. Phys. Lett. **100**, 113510 (2012).
[22] S. Carretta, A. Chiesa, F. Troiani, D. Gerace, G. Amoretti, and P. Santini, Phys. Rev. Lett. **111**, 110501 (2013).
[23] J. E. Healey, T. Lindstrom, M. S. Colclough, C. M. Muirhead, and A. Ya. Tzalenchuk, Appl. Phys. Lett. **93**, 043513 (2008).
[24] A. Palacios-Laloy, F. Nguyen, F. Mallet, P. Bertet, D. Vion, and D. Esteve, J. Low Temp. Phys. **151**, 1034 (2008); M. Sandberg, F. Persson, I. C. Hoi, C. M. Wilson, and P. Delsing, Phys. Scr. T **137**, 014018 (2009).
[25] Z. L. Wang, Y. P. Zhong, L. J. He, H. Wang, John M. Martinis, A. N. Cleland, and Q. W. Xie, Appl. Phys. Lett. **102**, 163503 (2013).
[26] M. A. Nielsen and I. L. Chuang, *Quantum Computation and Quantum Information* (Cambridge University Press, Cambridge, U.K., 2000).
[27] We note that there are N degenerate levels corresponding to one spin flip, but $|\psi_1\rangle$ is the only one which is strongly coupled to the cavity. The explicit form assumed here for $|\psi_1\rangle$ implies that all the spins have the same coupling to the corresponding photonic mode. However, the precise form of $|\psi_1\rangle$ is not important for the feasibility of the scheme.
[28] J.-Q. Liao, Z. R. Gong, L. Zhou, Y.-X. Liu, C. P. Sun, and F. Nori, Phys. Rev. A **81**, 042304 (2010).
[29] The third level of a superconducting qubit is exploited to implement a CZ gate, e.g., in Ref. [6].
[30] Y. Kubo, I. Diniz, A. Dewes, V. Jacques, A. Dréau, J.-F. Roch, A. Auffèves, D. Vion, D. Esteve, and P. Bertet, Phys. Rev. A **85**, 012333 (2012).
[31] We consider the superconducting qubit at the charge degeneracy point, in a regime $E_J \approx 6E_C$. Within this range of parameters, the spectrum is highly anharmonic. Hence, we can safely truncate the Hilbert space to the three lowest levels. In addition, we are close to the transmon regime, which ensures rather long dephasing times and $T_1^{CPB} \gg T_2^{CPB}$ [17, 32].
[32] J. Clarke and F. K. Wilhelm, Nature (London) **453**, 1031 (2008).
[33] D. L. Underwood, W. E. Shanks, J. Koch, and A. A. Houck, Phys. Rev. A **86**, 023837 (2012).
[34] M. Mariantoni, F. Deppe, A. Marx, R. Gross, F. K. Wilhelm, and E. Solano, Phys. Rev. B **78**, 104508 (2008).
[35] M. O. Scully and M. S. Zubairy, *Quantum Optics* (Cambridge University Press, Cambridge, U.K., 1997).
[36] H. Wang, M. Hofheinz, M. Ansmann, R. C. Bialczak, E. Lucero, M. Neeley, A. D. O'Connell, D. Sank, J. Wenner, A. N. Cleland, and John M. Martinis, Phys. Rev. Lett. **101**, 240401 (2008).
[37] The setup reported in Sec. IV is not straightforwardly scalable because increasing the number of qubits within a single cavity implies the use of an increasing number of distinct harmonics.
[38] R. E. George, J. P. Edwards, and A. Ardavan, Phys. Rev. Lett. **110**, 027601 (2013).
[39] An equation analogous to (17) holds also for a rotation of the second qubit, i.e., $\hat{R}_{zz}(\tau)[I \otimes \hat{R}_x(\varphi)]\hat{R}_{zz}(\tau) = I \otimes \hat{R}_y(\varphi)$. In that case, however, $\tau = \pi/4\delta_c$.
[40] P. Santini, S. Carretta, F. Troiani, and G. Amoretti, Phys. Rev. Lett. **107**, 230502 (2011).
[41] Even if tuning of the resonator harmonics might introduce extra dissipation to the photonic degrees of freedom, it has been shown that Q factors are preserved within a factor of 3 in the whole frequency modulation range [24]. We also point out that these effects are mainly attributed to thermal noise, which might be further reduced by working at lower temperatures and using high-frequency resonators, such as the ones assumed in the present work.
[42] T. C. Ralph and J. G. Pryde, Prog. Opt. **54**, 209 (2010).
[43] P. Kok, W. J. Munro, K. Nemoto, T. C. Ralph, J. P. Dowling, and G. J. Milburn, Rev. Mod. Phys. **79**, 135 (2007).
[44] M. Silva, M. Rötteler, and C. Zalka, Phys. Rev. A **72**, 032307 (2005).
[45] I. Diniz, S. Portolan, R. Ferreira, J. M. Gerard, P. Bertet, and A. Auffèves, Phys. Rev. A **84**, 063810 (2011).
[46] Z. Kurucz, J. H. Wesenberg, and K. Mølmer, Phys. Rev. A **83**, 053852 (2011).
[47] D. Gatteschi, R. Sessoli, and J. Villain, *Molecular Nanomagnets* (Oxford University Press, Oxford, U.K., 2006).
[48] M. Jenkins, T. Hümmer, M. J. Martínez-Pérez, J. García-Ripoll, D. Zueco, and F. Luis, New J. Phys. **15**, 095007 (2013).
[49] C. J. Wedge, G. A. Timco, E. T. Spielberg, R. E. George, F. Tuna, S. Rigby, E. J. L. McInnes, R. E. P. Winpenny, S. J. Blundell, and A. Ardavan, Phys. Rev. Lett. **108**, 107204 (2012).
[50] F. Troiani, D. Stepanenko, and D. Loss, Phys. Rev. B **86**, 161409(R) (2012).